Journal Pre-proofs

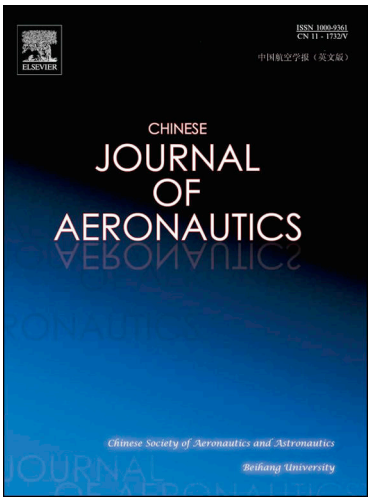

Cutting force and specific energy for rotary ultrasonic drilling based on kinematics analysis of vibration effectiveness

Zhen Li, Songmei Yuan, Jiang Ma, Jun Shen, Andre D.L. Batako

PII: S1000-9361(20)30586-0
DOI: https://doi.org/10.1016/j.cja.2020.12.023
Reference: CJA 1905

To appear in: *Chinese Journal of Aeronautics*

Received Date: 20 August 2020
Revised Date: 8 December 2020
Accepted Date: 8 December 2020

Please cite this article as: Z. Li, S. Yuan, J. Ma, J. Shen, A.D.L. Batako, Cutting force and specific energy for rotary ultrasonic drilling based on kinematics analysis of vibration effectiveness, *Chinese Journal of Aeronautics* (2021), doi: https://doi.org/10.1016/j.cja.2020.12.023

Contents lists available at ScienceDirect

Chinese Journal of Aeronautics

Journal homepage: www.elsevier.com/locate/cja

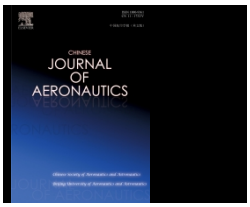

Cutting force and specific energy for rotary ultrasonic drilling based on kinematics analysis of vibration effectiveness

Zhen LI[a,b], Songmei YUAN[c,*], Jiang MA[a,*], Jun SHEN[a], Andre D. L. BATAKO[d]

[a]*College of Mechatronics and Control Engineering, Shenzhen University, Shenzhen, 518060, China*

[b]*College of Physics and Optoelectronic Engineering, Shenzhen University, Shenzhen, 518060, China*

[c]*School of Mechanical Engineering and Automation, Beihang University, Beijing, 100191, China*

[d]*The General Engineering & Technology Research Institute, Liverpool John Moores University, Liverpool L3 3AF, UK*

Received 19 August 2020; revised 24 September 2020; accepted 16 November 2020

Abstract

Rotary ultrasonic drilling (RUD) has become an effective approach for machining advanced composites which are widely using in the field of aeronautics. The cutting kinematics and the corresponding material removal mechanisms are distinct in different drilling areas during RUD. However, these fundamentals have not been fully considered in the existing studies. In this research, two distinct forms of interaction induced by ultrasonic vibration were considered as impact-separation and vibratory lapping between the abrasives and workpiece. And the conditions to guarantee the effectiveness of these interactions were obtained to eliminate diminishing effects of ultrasonic vibration. Based on indentation fracture theory, the penetration depth of abrasives and the axial drilling force model was derived for RUD. The verification tests of C/SiC composites resulted in a prediction error within 15%. Due to the minimal volume of material removed during each vibration cycle, the drilling force was more stable in vibration assisted mode. The specific drilling energy of RUD was firstly calculated based on the measured drilling load. It was found the drilling parameters should be matched with vibration frequency and amplitude to make better usage of the advantages of ultrasonic vibration, which is critical in the vibration assisted processing of advanced materials.

Keywords: Rotary ultrasonic drilling; Kinematics analysis; Vibration diminishing effect; Drilling force modelling; Specific drilling energy; Ceramic matrix composite

*Corresponding author. *E-mail address:* yuansmbuaa@163.com

1. Introduction

Ceramic matrix composites (CMC) have superior properties such as high specific strength, high specific rigidity, excellent oxidation and ablation resistance[1]. This makes CMC a kind of advanced material instead of the metals such as titanium alloy and superalloy used in the fields of aeronautics[2,3] astronautics[4], nuclear power[5], etc. The machining processes of CMC parts after the near-net-shape fabrication are still essential to achieve the desired surface quality and dimensional accuracy for application[6]. The hole drilling processes are generally needed to make mounting and locating holes for the specified parts like thermal protection tile on shuttle or brake pad for high

speed train and aircraft. However, the higher hardness, higher wear resistance and anisotropic properties are of great challenges, due to large drilling force, sever tool wear and hole defects in the conventional machining of CMC, as demonstrated in the study of CMC fracture mechanism and surface integrity[7,8]. These issues hampered the application of these advanced composites. Rotary ultrasonic machining (RUM) has become an effective approach for these materials to lower cutting load and improve surface quality. Pei, et al. proved the higher material removal rate and better surface quality in the RUM of ceramics[9], and Yuan, et al. achieved about 30% reduction of cutting force in the rotary ultrasonic side milling and surface milling of C/SiC composite[10,11], respectively. Therefore, various processes have been developed for the machining of specific geometry features of advanced materials based on RUM.

The technique of rotary ultrasonic machining has been studied for the difficult-to-machining materials including CMC, titanium alloy, and Inconel alloy[12,13]. Pei, et al. firstly studied the rotary ultrasonic drilling (RUD) of advanced ceramic using the core drill and developed a model of material removal under a constant feed force based on brittle fracture mechanism[14]. The influence of drilling parameters on material removal rates was extensively investigated in RUD[15], and a removal model under constant feed rate was developed[16]. Teti studied the machinability of different composites based on resin, metal and ceramic matrix, and pointed out that the machining of CMC are very challenging, even the polycrystalline diamond (PCD) tools experienced severe wear in short cutting time[17]. Therefore, the metal bonded diamond core drills are widely used in the practical machining of CMC. Here, the method of the material removal is by grinding away particles from the drilling area. Hocheng, et al. conducted the RUD of C/SiC composite and analyzed the influence of drilling parameters on the hole clearance, edge quality and tool wear, proving the advantages of RUD for CMC on the drilling quality and cost[18]. Li, et al. showed that the drilling force in the RUD of CMC could be decreased by 50% while increasing the material removal rate by 10%, comparing with the conventional drilling[19]. The spindle speed and feed rate and their interaction had significant effects on the hole exit quality. Ding, et al. also found a dramatically decrease of axial drilling force and torque in RUD of C/SiC[20], which aided the suppression of the edge chipping defects of holes. Wang, et al. studied the edge chipping mechanism of brittle materials in RUD[21], showing that the microcracks induced by ultrasonic impact in the drilling area can inhibit the propagation of large cracks, thus decreasing the chipping size of the drilled holes. To further improved the hole quality, a compound step-taper drill was designed[22], and longitudinal-torsional coupled vibration have been employed respectively in RUD[23,24]. The critical drilling force was investigated to guarantee the effectiveness of ultrasonic vibration during RUD[25]. The deep-hole grinding process assisted by ultrasonic vibration has also been developed for ceramics to reduce the exit edge-chipping[26]. Also, the high frequency vibration was found facilitating the brittle-to-ductile transition[27], which is conducive for the brittle materials to suppress cracks during machining[28]. In addition to the improvement of drilling quality, efficiency and tool life, Cong, et al. found that the energy consumption of ultrasonic vibration system accounted only for about 9% of the total processing energy consumption in the RUD[29]. Islam, et al. developed a drilling load model to predict the drilling force and torque for the RUD of C/SiC based on brittle fracture removal mode[30], and the model agreed well with the test results in a certain range of drilling parameters. However, the influence of the distinct kinematics of abrasive in different drilling areas, and the corresponding vibration effectiveness in RUD have not been studied.

From the review above, most of the previous research works focused on the influence of drilling parameters on the drilling efficiency, hole quality, and tool life in the RUD. It was found that chipping defect was mainly caused by the fracture of the thin material layer at the hole exit, due to the thrust of the axial drilling force, and the parameters optimization was generally carried out based on experiments. However, only a few studies are devoted to the fundamental principles, such as vibration diminishing effect and drilling force control in the RUD of CMC, especially, the distinct kinematics of abrasives in different drilling areas, and the conditions to guarantee vibration effectiveness have not been considered in the previous research, and the specific drilling energy have not yet been studied, which are critical for the process design of the RUD of advanced materials. Since the interaction between abrasives and workpiece directly affects the material removal mechanism and drilling load magnitude, there is a need to eliminate the diminishing effect of ultrasonic vibration, develop a drilling force model and analyze the specific drilling energy based on the kinematics of RUD for CMC.

This paper studied the kinematics of the abrasives in different cutting areas of the core drill, including the cylindrical surface, end surface, and chip flute edge in RUD. The interactions between abrasives and workpiece under ultrasonic vibration were analyzed including the impact-separation and vibratory lapping. And the conditions to guarantee the effectiveness of these interactions were also obtained to eliminate the diminishing effects of ultrasonic vibration during RUD. The penetration depth of abrasives in different drilling areas during RUD were calculated based on indentation fracture theory, and the axial drilling force model was developed considering the loads produced from different drilling areas. The RUD experiments of C/SiC were conducted for the verification of

the drilling force model. And the specific drilling energy was then calculated and discussed based on the measured drilling load. This research can provide a guidance for the design and optimization of vibration assisted processing of advanced materials.

2. Kinematics analysis of RUD

Vibration assisted machining is a well-known technique that is used in various industry. High and low frequency vibration introduced in the cutting areas significantly changes the relative cutting motion between the cutting tool and workpiece and subsequently the material removal mechanisms, comparing to the conventional machining. Although additional energy is input into the vibratory, the energy consumption of vibration system generally makes up a very small portion of the total energy requirement of machining. However, the introduction of vibration substantially decreases the specific machining energy, as proved by Batako, et al.[31]

Referring to the aspects of energy input and the machining kinematics, the positive effects and benefits accrued by superimposing vibration on the machining, the efficiency and the quality of the product are attributed to the changes in the kinematics in the cutting areas rather than the minute additional energy of the vibration system. Typically, the power of the systems for superimposing vibration is in the range of a few hundred Watts, whereas the machining and the machine tools are operating in the range of tens of kilo Watts. This ratio of power requirement illustrates the improvement brought by vibratory machining is not due to additional power input, yet due to a radical change in the kinematics and the impulsive interaction between the tool and the medium been treated. Therefore, the analysis of the kinematics and fundamental understanding of the interactions in vibratory cutting is critical in mastering and exploiting widely all the applications. This understanding would allow the optimization all vibratory machining processes and maximizing the benefits accrued by the synergy of vibro-impact processes in RUD. Fig. 1(a) and Fig.1(b) shows a core drill with diamond bonded abrasives on the cylindrical and tip surfaces generally used in RUD. The chip flutes were incorporated on the tip of the core drill to prevent clogging and chip evacuation from the relatively closed drilling areas. This is important to avoid the drilling failure for the difficult-to-machining materials like C/SiC. The ultrasonic vibration of a sine wave was applied in the axial direction with a frequency of 16 kHz to 50 kHz. Therefore, the displacement of the drilling tool during RUD is a combination of rotational motion of the spindle at a speed S (rpm), a vertical down motion at a feed rate v_f (mm/min), and the ultrasonic oscillation along the tool axis. The simulated trajectories of one single diamond grain on the surface of the drill in RUD and in conventional drilling (CD) are shown in Fig.1(c).

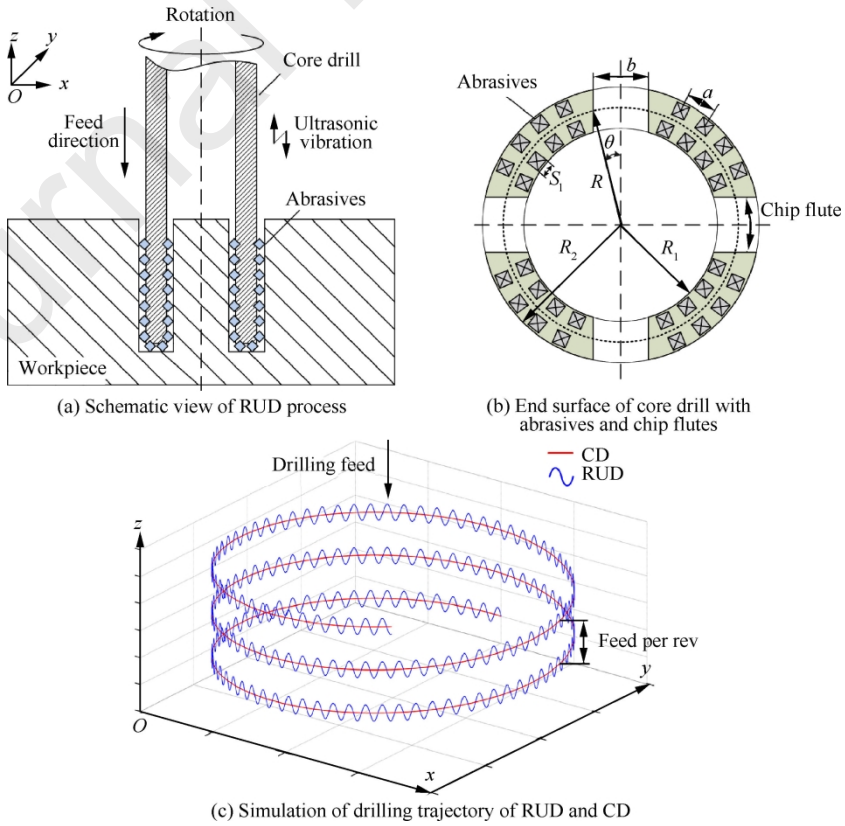

(a) Schematic view of RUD process

(b) End surface of core drill with abrasives and chip flutes

(c) Simulation of drilling trajectory of RUD and CD

Fig. 1. Processing principle and kinematics of RUD.

The equation of motion of individual abrasive grains on the drilling tool is expressed as:

$$S_{\mathrm{RUD}}(t)=\begin{bmatrix} S_x = R\cos(\omega t) \\ S_y = R\sin(\omega t) \\ S_z = -A\sin(2\pi f t+\varphi_0)-v_{\mathrm{f}}t \end{bmatrix} \tag{1}$$

where R is the radius of the core drill, ω is the angular velocity of the spindle rotation and can be defined as $\pi S/30$, t is the machining time, A is the ultrasonic vibration amplitude, f is the ultrasonic vibration frequency, φ_0 is the initial phase of ultrasonic vibration.

Thus, the cutting velocity of abrasive grains on the core drill can be deduced as:

$$V_{\mathrm{RUD}}(t)=\frac{\mathrm{d}S_{\mathrm{RUD}}}{\mathrm{d}t}=\begin{bmatrix} V_x = -R\omega\sin(\omega t) \\ V_y = R\omega\cos(\omega t) \\ V_z = -2\pi f A\cos(2\pi f t+\varphi_0)-v_{\mathrm{f}} \end{bmatrix} \tag{2}$$

It can be seen from the equations of motion and the simulated drilling trajectory that the cutting velocity and the length of the abrasive grain trajectory is greater in RUD, due to the superimposed ultrasonic vibration into the process. This means that each cutting edge travels a longer distance, thus cutting more and removing more material than in conventional mode. Though the motion of abrasives is identical in the same system of coordinates, the interactions between abrasives and workpiece material are distinct in different drilling areas. The distribution of abrasives on core drill directly determines the interaction mode relative to the workpiece in RUD.

2.1. Vibratory lapping effect in cylindrical drilling area

For the abrasives on the cylindrical surface of the core drill, the ultrasonic vibration is parallel to the hole wall and perpendicular to the rotary cutting direction in RUD, thus the abrasives have a continuous contact with the workpiece and reciprocating vibratory motion in this drilling area. A minimum volume of material is removed on the hole wall, and the drilling load produced from this area generally can be ignored in the machining of the hard and brittle materials with little deformation. The rubbing and frictional oscillatory motion of the abrasives on the cylindrical surface induces a finishing lapping process which is crucial in improving the surface quality of the hole wall (Fig. 2).

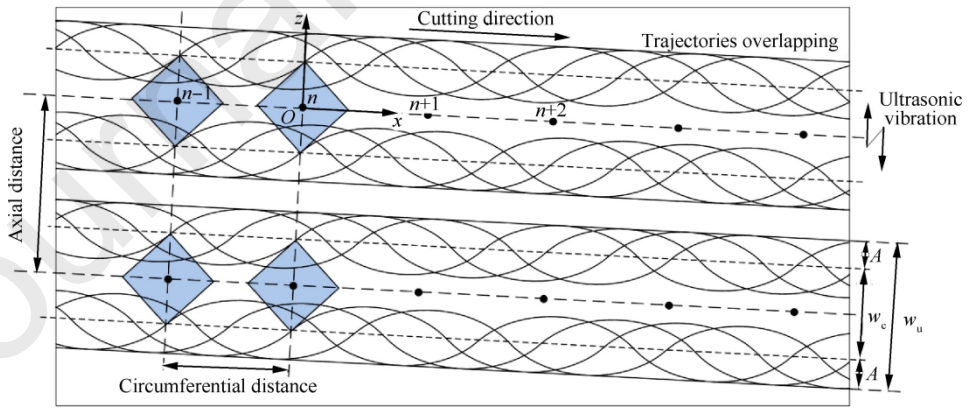

Fig. 2. Vibratory lapping effect of abrasives on cylindrical drilling area.

To analyze the cutting kinematics, the hole wall is unfolded to a plane surface as shown in Fig. 2, the abrasives vibrate around the conventional scratching trajectory, thus the scratching width of the abrasives is increased by twice amplitude of ultrasonic vibration. The trajectories of the abrasives circumferentially distributed on the core drill will be crossed and superposed in the cutting area along with the cutting motion, leading to a polishing/lapping effect on the hole wall. The scratching direction on the material by abrasives was adopted as positive in the direction of X axis in Fig. 2. Choosing one of the abrasives (n) in the cylindrical drilling area as the reference point, the trajectory equation can be expressed relative to Z axis as:

$$z_n = A\sin(\frac{2\pi f}{\sqrt{v_f^{\ 2} + v_c^{\ 2}}}x) \tag{3}$$

Due to the circumferential distance between the abrasive grains, there is a time lag in the cutting motion of the subsequent abrasives, causing the phase difference of the trajectories of the circumferentially adjacent abrasives. This phase can be expressed as:

$$\phi_0 = \frac{2\pi f a}{\sqrt{v_f^{\ 2} + v_c^{\ 2}}} \tag{4}$$

where v_c is the rotary cutting speed which can be expressed as $\pi SR/30$, a is the circumferential distance between the adjacent abrasives.

Supposing that the abrasives are evenly distributed on the cylindrical drilling area, the axial feed lag of the circumferentially adjacent abrasives can be considered as the feed per revolution divided by the total number of the circumferential abrasives and expressed as:

$$z_0 = \frac{v_f a}{2\pi RS} \tag{5}$$

Thus, the overlapping condition of cutting trajectories of abrasives can be deduced as:

$$z_{n+m} = A\sin(\frac{2\pi f}{\sqrt{v_f^{\ 2} + v_c^{\ 2}}}x - m\phi_0) + mz_0 \tag{6}$$

where m is the number of abrasives grains from (n+m) to the reference point (n), the positive m means the abrasive in front of point (n) and the negative m means the subsequent abrasive.

To achieve better surface quality of the hole wall, a dense overlapping of the cutting trajectories is desired. Therefore, it can be seen from the kinematics analysis of cutting trajectories overlapping in Eq.(6) that increasing the vibration frequency and amplitude will increase the density of overlapping trajectories or decreasing the rotary cutting speed and the adjacent distance of abrasives will induce the desired lapping/polishing effect, due to close packed intersections and superpositions of cutting trajectories. Consequently, this process will produce a fine finishes surface, which is inherent to vibration assisted machining and in this case of RUD.

2.2. Intermittent machining in bottom drilling area

Since, the ultrasonic vibration and the feed direction are vertical to the bottom drilling area, thus the abrasive grains located at the tip surface of the drill periodically penetrate into and disengage from the workpiece material at high frequency. The material is mainly removed by abrasives at the tip surface and the major drilling load is also located on this drilling area. This intermittent cutting mode is the essence of vibratory cutting and especially in machining hard and brittle materials, because it significantly reduces the cutting force and improve the hole exit quality. Therefore, achieving the intermittent machining in the bottom drilling area is crucial for a better usage of the advantages of ultrasonic vibration in RUD.

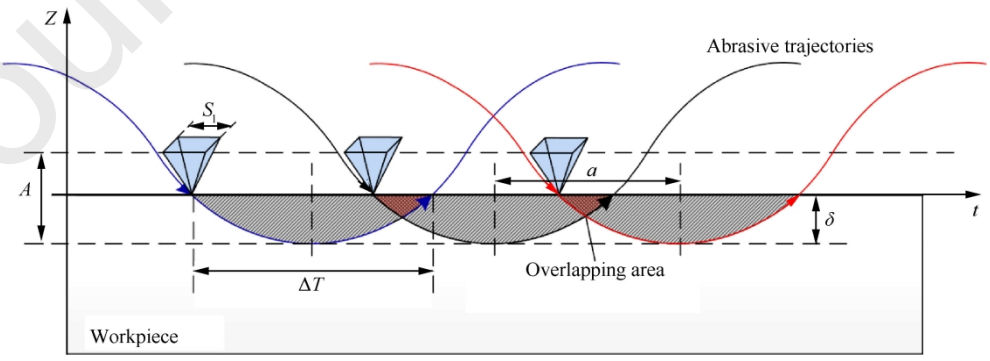

Fig. 3. Intermittent cutting behavior of abrasives on bottom drilling area.

As shown in Fig. 3, the abrasives at the tool tip surface impact into the material for an effective cutting time ΔT and then separate from the drilling area, so the impact depth of the abrasive grains increase from zero to δ along

with the drilling motion, and reach to the maximum value at the vibration peak. The periodical time involved in cutting during one vibration cycle can be expressed as:

$$\Delta T = \frac{(\pi - \arccos(\delta/A - 1))}{\pi f} \tag{7}$$

The abrasives cut the material by impact and scratching for a short time ΔT, and the chips are formed and removed in each vibration cycle. According to the vibration frequency (f), the impact times within 1 s is f, and the corresponding cutting length by the spindle rotation can be expressed as $\pi SR/30$, here, S is the spindle speed (r/min), R is the radius of the core drill (mm). Therefore, the number of impacts per unit cutting length can be expressed as:

$$n = \frac{f}{R \cdot \omega} = \frac{30f}{\pi SR} \tag{8}$$

This implies that, the high frequency the more chips will be formed due to the impact, which, indicates that the chip size will be much smaller than the conventional machining due to the hammering process. The smaller the chips are, the easier is their evacuation form the cutting zone and the less clogging occurs. Since the cutting zone and the tool are cleared from debris, the cutting process is much efficient due less friction aided by the intermittent cutting which imparts low cutting forces. In addition, the propagation of cracks in the drilling area are constrained in a smaller range due to the nibbling/pecking material removal process in each vibration cycle, and this leads to reduced defects in the machined part. In this type intermittent cutting, each single abrasive will leave some material behind which will be removed by the following abrasives, subsequently clearing and removing cracks formed earlier. To improve the material removal rate in the cutting area, the scratching grooves between the adjacent abrasives should be partially overlapped during the intermittent cutting, as shown in Fig. 3 To achieve this, the following condition should be met $v_c \Delta T > a$, that is:

$$SR(\pi - \arccos(\delta/A - 1)) > 30af \tag{9}$$

where a is the circumferential distance between the adjacent abrasives at the tool tip surface. δ is the maximum penetration depth and can be approximated as the feed per revolution divided by the total number of active abrasive grains on the cutting tip of the drilling tool, that is $v_f a/2\pi SR$.

It can be seen from Eq.(9) that increasing the vibration frequency and the cutting velocity as well as the drilling feed lead to an increased material removal in the intermittent machining. However, when the cutting speed increases, the number of impacts in the unit cutting length decreases, as shown in Eq.(8). The reduction of number of impacts per unit length is not desired here as it lessens the vibro-impact effect, which is the prime aim of introducing the vibration in the cutting. The ratio of spindle speed (S) to vibration frequency (f) should be considered in the cutting parameter optimization during ultrasonic machining.

The effectiveness of intermittent machining is characterized by impact-separation in the drilling area, which is a function of the drilling parameters. In Fig. 3, setting the direction of penetration depth in negative Z axis, the drilling trajectory of the first abrasive grain (z_1) impacting into the material followed by the subsequent abrasive (z_2) can be expressed as:

$$\begin{cases} z_1 = A\sin(2\pi f t + \varphi_0) - v_f t \\ z_2 = A\sin(2\pi f (t + \Delta t) + \varphi_0) - v_f (t + \Delta t) \end{cases} \tag{10}$$

where Δt is the time lag between the adjacent abrasive grains at the tip surface of the core drill.

The dynamic impact depth of the abrasive grain into the medium can be considered as the result of the superposition of the drilling trajectories of the two adjacent grains:

$$\Delta z = z_2 - z_1 = -v_f \Delta t + 2A\sin(\pi f \Delta t)\cos(2\pi f \cdot (t + \Delta t/2) + \varphi_0) \tag{11}$$

To achieve the impact-separation behavior, the dynamic penetration depth should periodically switch between a positive and negative value that is $\Delta z > 0$ for half period and $\Delta z < 0$ for the second half. This alternation induces an interrupted contact-indentation-cutting process, which is inherent to intermittent machining. The equation should have solutions of real numbers when Δz is equal to zero, achieving that the abrasives fully separate from the processed medium, the motion should satisfy the following relations:

$$v_f \Delta t \le \left| 2A\sin(\pi f \Delta t) \right| \tag{12}$$

Due to the chip flutes on the end surface of core drill with a width of b, as shown in Fig. 1b, the distance between the adjacent abrasives distributed on the end surface and the chip flute edge is different, thus the corresponding lag time can be respectively expressed as:

$$\begin{cases} \Delta t_{\mathrm{a}} = \dfrac{a}{v_{\mathrm{c}}} = \dfrac{30a}{\pi SR} \\ \Delta t_{\mathrm{b}} = \dfrac{2\theta}{\omega} = \dfrac{60\arcsin(b/2R)}{\pi S} \end{cases} \tag{13}$$

The solution of Eq.(12) and Eq.(13) leads to the expression of the condition to achieve the intermittent machining in RUD:

$$\begin{cases} v_{\mathrm{f}} \le \dfrac{\pi SAR}{15a}\left|\sin(\dfrac{30a\,f}{SR})\right| \\ v_{\mathrm{f}} \le \dfrac{\pi SA}{30\arcsin(b/2R)}\left|\sin(\dfrac{60\,f\arcsin(b/2R)}{S})\right| \end{cases} \tag{14}$$

Therefore, there are two distinct interaction forms including vibratory lapping and impact-separation in the different drilling areas, which significantly influence the material removal mechanism. It is crucial to achieve these interaction forms in cutting zone to ensure the efficiency of the introduced ultrasonic vibration, aiming at reducing cutting forces and improving machining quality. The drilling parameters should be matched with vibration amplitude and frequency based on Eqs.(6), (9) and (14) to eliminate the diminishing effects of ultrasonic vibration.

3. Development of drilling force model

The drilling load is mainly produced by the intermittent cutting of abrasives distributed at the tool tip surface and the chip flute edge. According to the indentation theory, the elasto-plastic zone will firstly appear at the cutting edges when the abrasives impact into the target material. As the further increase of impact depth, the median cracks are initiated, and then generating the lateral cracks, which propagate and cross with other neighbouring cracks inducing the spalling of the workpiece material as illustrated in Fig. 4, $\delta_{\max}$ is the maximum impact depth, C_{d} is the depth of material removed by fracture, α is the half angle of the grains, C_{l} is the length of lateral cracks, C_{h} is the depth of lateral cracks, w is the half of the impact width. Therefore, the workpiece material is mainly removed by the impact and sweeping of abrasives in the drilling area, the removing processes can be formed by two parts due to the lateral crack propagation: the sweeping zone with the maximum impact depth ($\delta_{\max}$), and the cracking zone with the brittle fracture depth (C_{d}).

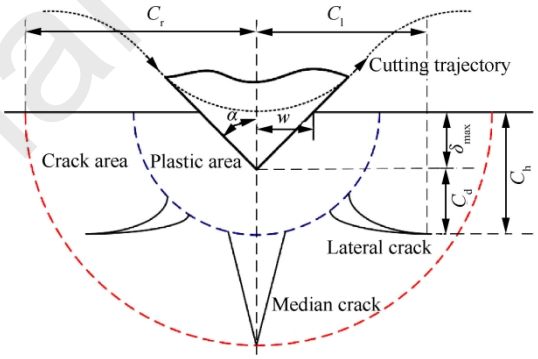

Fig. 4. Elastic-plastic deformation and crack propagation in drilling area.

In the stable stage of drilling, the undeformed chip thickness (h_{m}) in the cutting area can be considered consist of impact depth and brittle facture depth[32]:

$$\begin{cases} h_{\mathrm{m}} = \delta_{\max} + C_{\mathrm{d}} = C_{\mathrm{h}} \\ C_{\mathrm{h}} = C_0 \tan\alpha^{-1/3}(E^{1/2}/H_{\mathrm{v}})(F)^{1/2} \\ C_{\mathrm{l}} = C_0 \tan\alpha^{-5/12}(E^{3/4}/(H_{\mathrm{v}}K_{\mathrm{IC}}(1-\nu^2)^{1/2}))^{1/2}(F)^{5/8} \end{cases} \tag{15}$$

where C_0 is a constant that independent of material/indenter system, C_0=0.226. F is the indentation force.

The indentation geometry relation in Fig. 4 can be expressed as[33]:

$$\begin{cases} \delta_{\max} = \dfrac{w}{t\tan\alpha} \\ \left(\dfrac{K_{\mathrm{IC}}}{H_{\mathrm{v}} w^{1/2}}\right)\left(\dfrac{H_{\mathrm{v}}}{E}\right)^{2/5} = c_1 \left(w / C_{\mathrm{h}}\right)^{c_2} \end{cases} \tag{16}$$

where K_{IC} is the fracture toughness of the material, H_{v} is the Vikers-hardness, E is the elastic modulus, c_1 and c_2 are constant coefficient, c_1=2.88, c_2=0.25.

The solution of Eq.(15) and Eq.(16) gives the equation of maximum impact depth:

$$\delta_{\max} = 0.243 \frac{h_{\mathrm{m}}^{1/3}}{\tan\alpha}\left(\frac{K_{\mathrm{IC}}}{H_{\mathrm{v}}^{3/5} E^{2/5}}\right)^{4/3} \tag{17}$$

The undeformed chip thickness (h_{m}) is subsequently calculated from the tool feed, the lag time (Δt) between two adjacent abrasives at the tool tip surface and the chip flute edge. The change of cutting depth in different drilling area during RUD is shown in Fig. 5. From the entering stage, the cutting depth gradually increases along with the rotation and feed motions, then reaching to the stable drilling stage with a stable cutting depth. The cutting depth gradually decreases in the exiting stage, but due to the thrust of the axial drilling force, the workpiece material near the hole exit fractures before the cutting depth deceasing to zero. Consequently, the prediction and control of the drilling force in the stable drilling stage is crucial to reduce the chipping size of the hole exit. The cutting depth of the abrasives on the chip flute edge is generally larger than that of the abrasives at the tool tip surface, and the corresponding drilling load produced at the flute edge also need be taken into consideration in modelling the drilling force.

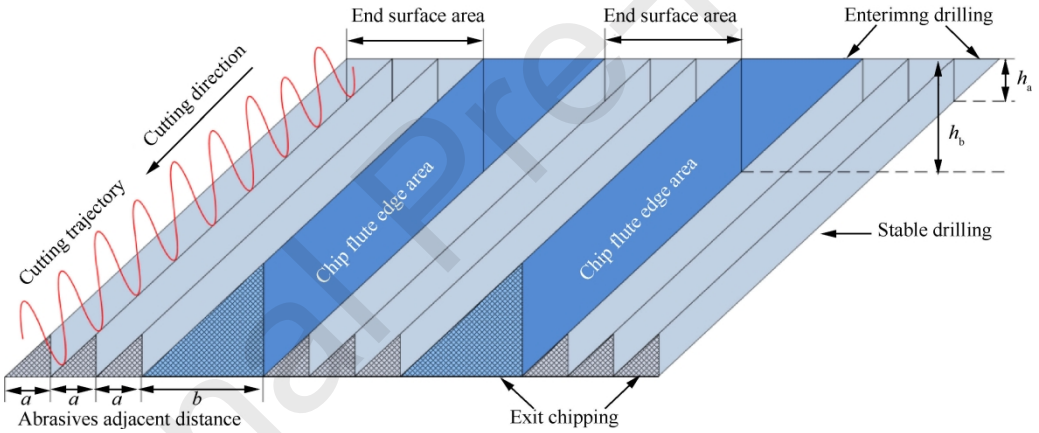

Fig. 5. Change of abrasive penetration depth in different drilling areas.

In Fig. 1(b), one could assume that the abrasive grains are distributed orderly in n concentric circles from the inner radius (R_1) to the outer radius (R_2). It is crudely assumed that the abrasives are distributed uniformly along the circumference on each successive circle with a radius of (R_1+na). With the distance between two neighboring abrasives at the tool tip surface being a, and n=0, 1, 2,…, N, so N=(R_2−R_1)/a. Therefore, considering the kinematic analysis in Eq.(13), the undeformed chip thickness (h_{a}) for each abrasive at the tool tip and on the flute edge (h_{b}) can be expressed as:

$$\begin{cases} h_{\mathrm{a}} = v_{\mathrm{f}} \Delta t_{\mathrm{a}} = \dfrac{30 a v_{\mathrm{f}}}{\pi S (R_1 + na)} \\ h_{\mathrm{b}} = v_{\mathrm{f}} \Delta t_{\mathrm{b}} = \dfrac{60 \mathrm{v}_{\mathrm{f}} \arcsin(b/2(R_1 + na))}{\pi S} \end{cases} \tag{18}$$

The abrasives are bonded on the end surface of the tool by electrodeposition, and the adjacent distance is mainly controlled by the mesh size and concentration of the abrasives. To evaluate the mean adjacent distance (a) for the cutting force modelling, the abrasives are assumed to distribute uniformly and in order in the cutting areas as shown in Fig. 1(b). The diamond abrasive concentration is defined as the mass of abrasive per unit volume within working layer. In practical and industrial terms, a 100% concentration is defined as per cubic centimeter

volume of abrasive grains containing 4.4 karats. Based on this definition, the total number of diamond abrasives involved in cutting area was expressed as[11]:

$$N_\alpha = \left(\frac{0.88\times10^{-3}}{\left(\sqrt{2}/3\right)S_1^3\cdot\rho} \cdot \frac{C_\alpha}{100} \right)^{2/3} \cdot A_0 \tag{19}$$

where, S_1 is the side length of the abrasive (220 μm) which can be obtained from the standard mesh size (60#), ρ is the density of diamond (3.52×10^{-3} g/mm^3), C_α is the concentration of abrasive grains distributed on the core drill, A_0 is the active area of tool involved in cutting.

The nominal area of a single diamond abrasive can be deduced as:

$$A_s = a^2 = \frac{A_0}{N_\alpha} \tag{20}$$

where a is the distance between two adjacent abrasives at the tool tip surface, and the solution of Eq.(19) and Eq.(20) leads to the expression as:

$$a = \left(\frac{0.88\times10^{-3}}{\left(\sqrt{2}/3\right)S_1^3\cdot\rho} \cdot \frac{C_\alpha}{100} \right)^{-\frac{1}{3}} = 5.73S_1C_\alpha^{-1/3} \tag{21}$$

a can be calculated as about 1200 μm, and the space between adjacent abrasives is about 900 μm.

The substitution of Eq.(18) and Eq.(21) into Eq.(17), provides the maximum impact depth of abrasive grains at the tool tip surface (δ_a) and at the flute edge (δ_b):

$$\begin{cases} \delta_a = 1.35\left(\dfrac{K_{IC}}{H_v^{3/5}E^{2/5}} \right)^{4/3} \left(\dfrac{S_1 v_f}{\pi S(R_1 C_\alpha^{1/3} + 5.73nS_1)} \tan^{-3}\alpha \right)^{1/3} \\ \delta_b = 0.955\left(\dfrac{K_{IC}}{H_v^{3/5}E^{2/5}} \right)^{4/3} \left(\dfrac{v_f \arcsin(b/2(R_1 + 5.73nS_1C_\alpha^{-1/3}))}{\pi S} \tan^{-3}\alpha \right)^{1/3} \end{cases} \tag{22}$$

With respect to the impact-separation in intermittent cutting, the dynamic penetration depth of an abrasive in one vibration cycle as shown in Fig. 6, the abrasive comes in contact with the workpiece material at a time t_1 for (δ=0). Subsequently, along with the cutting motion, the abrasive penetrates deeper into the medium up to the maximum ($\delta=\delta_{mn}$) at the vibration peak (t=1/2f). Then, the abrasive disengages gradually to (δ=0) at a time t_2.

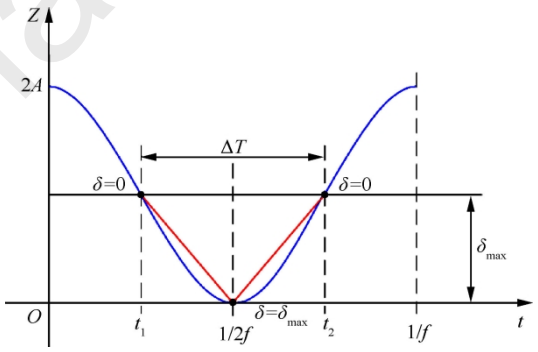

Fig. 6. The impact and sweeping trajectory in a single vibration cycle

The dynamic changing of impact depth during the contact time (ΔT) can be given as:

$$\begin{cases} \delta = \delta_{\max} - \left(A\cos(2\pi f t) + A \right) & t \in [t_1, t_2] \\ t_1 = \dfrac{\arccos(\delta_{\max}/A - 1)}{2\pi f} \\ t_2 = \dfrac{2\pi - \arccos(\delta_{\max}/A - 1)}{2\pi f} \end{cases} \tag{23}$$

By simplifying the penetration trajectory into straight lines marked red as shown in Fig. 6, the Eq.(23) can be redefined as:

$$\begin{cases} \delta = \dfrac{\delta_{\max}}{1/2f - t_1} t - \dfrac{\delta_{\max}}{1/2f - t_1} t_1 & t \in \left[t_1, \dfrac{1}{2f} \right] \\ \delta = \dfrac{\delta_{\max}}{1/2f - t_2} t - \dfrac{\delta_{\max}}{1/2f - t_2} t_2 & t \in \left[\dfrac{1}{2f}, t_2 \right] \end{cases} \tag{24}$$

The instantaneous drilling force F_n' during the impact cycle can be expressed as:

$$F_n' = 4k \frac{\tan\alpha}{\cos\alpha} \cdot H_v \cdot \delta^2 \tag{25}$$

k is a correlation coefficient for the geometrical irregularity and uneven distribution of abrasives.

Thus, the impulse of the drilling force during one ultrasonic vibration cycle is deduced as:

$$I = \int_0^{1/f} F_n' \mathrm{d}t = \int_{t_1}^{t_2} F_n' \mathrm{d}t \tag{26}$$

The substitution of Eq.(24) and Eq.(25) into Eq.(26), gives:

$$I = 2\int_0^{\delta_{\max}} 4k \frac{\tan\alpha}{\cos\alpha} H_v \delta^2 \left(\frac{1/2f - t_1}{\delta_{\max}} \right) \mathrm{d}\delta = \frac{8}{3} k \frac{\tan\alpha}{\cos\alpha} H_v (1/2f - t_1) \delta_{\max}^2 \tag{27}$$

The average drilling force (F_n) of an abrasive grain within one vibration cycle can be given as:

$$F_n = If = \frac{4k}{3\pi} \cdot \frac{\tan\alpha}{\cos\alpha} H_v \left(\pi - \arccos\left(\frac{\delta_{\max}}{A} - 1 \right) \right) \delta_{\max}^2 \tag{28}$$

Due to the gap occupied by the flutes on the drill, the number of abrasives at the tip surface is reduced. Consequently, the number of abrasives M_n distributed on each circle with a radius of (R_1+na) is redefined in Eq.(29), where N_c is the number of flutes on the drill:

$$M_n = \frac{(2\pi - 2N_c \arcsin(b/2(R_1 + 5.73nS_1 C_\alpha^{-1/3})))(R_1 C_\alpha^{1/3} + 5.73nS_1)}{5.73S_1} \tag{29}$$

Combining Eq.(22), Eq.(28), and Eq.(29), the cutting force produced by the abrasives at the tool tip surface, is estimated as follows:

$$F_a = \sum_{n=0}^{N} \frac{4k}{3\pi} \cdot \frac{\tan\alpha}{\cos\alpha} H_v M_n \left(\pi - \arccos\left(\frac{\delta_a}{A} - 1 \right) \right) \delta_a^2 \tag{30}$$

And the cutting force produced by the abrasives on the chip flute edges can be expressed as:

$$F_b = N_c \sum_{n=0}^{N} \frac{4k}{3\pi} \cdot \frac{\tan\alpha}{\cos\alpha} H_v \left(\pi - \arccos\left(\frac{\delta_b}{A} - 1 \right) \right) \delta_b^2 \tag{31}$$

N, as defined above, is the number of concentric circles of abrasives on the end surface, and can be derived from Eq.(21) giving, N= 0.175 $(R_2 - R_1) S_l^{-1} C_\alpha^{1/3}$.

Therefore, the axial drilling force F during RUD is the sum of the cutting force of all active abrasive involved in the bottom drilling area, i.e. F=F_a+F_b. The solutions of Eq.(22), Eq.(30), and Eq.(31) lead to a set of simultaneous equations for the axial cutting force of RUD.

4. Experimental work

The experimental setup is shown in Fig. 7. The drilling tests for were performed on a 3-axis vertical machining center (HAAS Mini mill), mounting with an in-house designed ultrasonic device on the spindle. The experimental

apparatus had four parts: an ultrasonic vibration system operating at a frequency of 17 kHz with the amplitude of 5 μm, a core drill with four chip flutes, a 3-axis dynamometer for force measurement (9257B, Kistler), and C/SiC workpieces with a size of 95 mm×40 mm×5 mm. The mechanical properties of the C/SiC (CHAOMA Technology Co., Ltd, Xi'an, China), and the parameters of the core drill are given in Table 1 and Table 2, respectively. The C/SiC samples were fabricated by carbon fiber weave, vapor deposition, liquid phase deposition and carbonization. In order to prevent the infiltration of coolant into the composites and causing material performance degradation, the dry conditions were undertaken for the drilling tests of C/SiC. Based on the kinematic analysis of RUD in Section 2, the maximum vibration amplitude (5 μm) was adopted, and adequate machining parameters were selected as illustrated in Table 3.

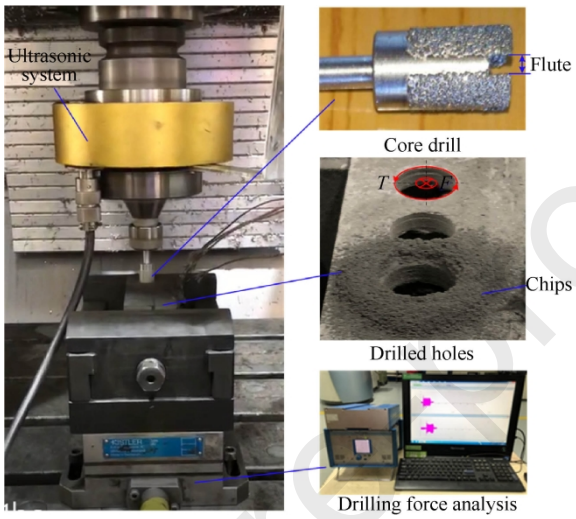

Fig. 7. Experimental setup for RUD.

Table 1 Mechanical properties of C/SiC.

Parameters	Value
Density (ρ)	2.0 g/cm3
Porosity (v)	17%-20%
Tensile strength (σ_t)	≥ 40 MPa
Surface shear strength (σ_c)	≥ 10 MPa
Compression strength(σ_y)	590 MPa
Elastic modulus (E)	67.7 GPa
Fracture toughness (K_{IC})	17.9 MPa·m$^{1/2}$
Vickers-hardness (H_v)	9.7 GPa

Table 2 Parameters of the core drill.

Parameters	Type
Abrasive	Diamond
Bond type	Brazing
Grain size	60#
Concentration	C_α=100
Inner radius	R_1=5 mm
Outer radius	R_2=6 mm
Chip flute width	b=2 mm

5. Results and discussion

5.1. Drilling force model verification

A set of experiments for RUD of C/SiC was undertaken to validate the drilling force model developed in Section 3. The drilling process can be divided into three stages: entering, stable, and exiting, as shown in Fig. 8. The measured axial drilling force was the average value during the period of stable stage. It is seen that the drilling

force in the RUD was lower than the conventional drilling without ultrasonic vibration. In addition, the conventional drilling force of C/SiC showed a strong fluctuation because of the material heterogeneity induced by the reinforced layers of the carbon fiber textile in the feed direction, while the drilling force in RUD tended to be more stable, due to the minimal volume of material removal during each vibration cycle.

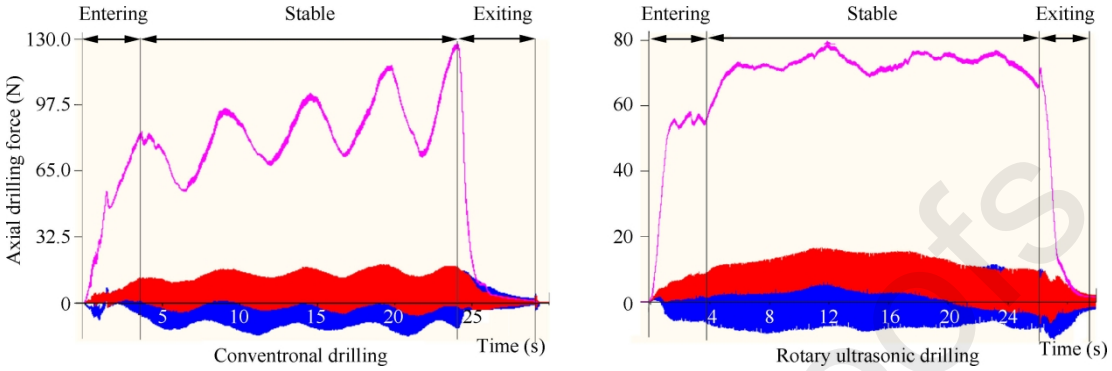

Fig. 8. Drilling force measurement and comparison (S=1000 r/min, v_f =10 mm/min).

The actual measured drilling forces (F_m) were compared with the simulation values (F_s') calculated from the developed drilling force model without k to define the correction coefficient k. The least square method was adopted to calculate the k value for the drilling force correction. Here, several iterations were undertaken using the data from the preliminary experiments and applying the formula $\sum(F_m - kF_s')^2$ to reach a minimum value of k =1.65. After defining k, ten experiments were undertaken using the machining parameters illustrated in Table 3. The results obtained here were used to verify the cutting force model. A comparison of measured and simulated values of drilling force was undertaken to verify the efficiency of the model.

Table 3 Axial drilling force data from experiments and simulation.

Test No.	Spindle speed S (r/min)	Feed rate v_f (mm/min)	Drilling force (N) F_m (measured)	Drilling force (N) F_s (simulation)	Error $(F_s-F_m)/F_m$
1	1000	40	178.5	202.1	13.22%
2	2000	40	120.3	130.3	8.31%
3	3000	40	103	97.3	-5.53%
4	4000	40	94.5	82.5	-12.70%
5	6000	40	77.1	63.4	-17.77%
6	4000	10	27.7	30.4	9.75%
7	4000	20	58.2	52.3	-10.14%
8	4000	60	125.3	105.1	-16.12%
9	4000	90	158.6	135.9	-14.31%

The variation of the measured and simulated drilling forces along with spindle speed and feed rate is illustrated in Fig. 9 and Fig. 10. It is seen that the drilling force decreased with the increase of spindle speed, but it increased with the increase of feed rate. These results agree well with the kinematics analysis of RUD in Section 2. When the spindle speed or cutting velocity increases, the time lag between the motions of two adjacent abrasives decreases, inducing the reduction of the cutting thickness of the abrasives in the drilling area, thus the drilling force decreases. Whereas with the increase in feed rate, the penetration depth into the workpiece material by abrasives increases, producing larger drilling load during RUD. The error of drilling force between modelling and experiments is below 15 %, except Test 5 (-17.77%) and Test 9 (-16.12%). These discrepancies are mainly attributed to the inhomogeneous and anisotropic properties of C/SiC composites. However, by averaging the discrepancies across all experiments one could get an overall error of 5.7%.

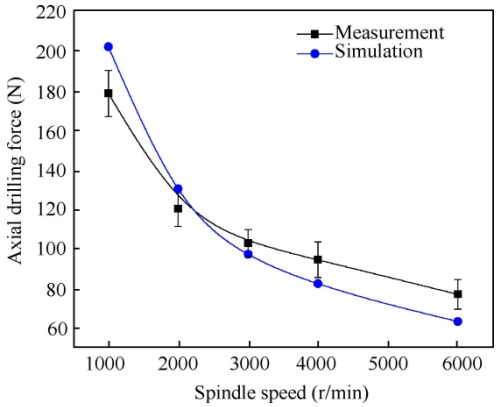

Fig. 9. Relationship between drilling force and spindle speed (v_f=40 mm/min) .

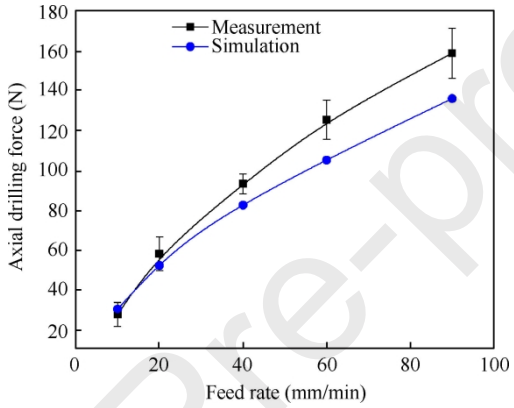

Fig. 10. Relationship between drilling force and feed rate (S=4000 r/min).

From the micro-perspective of material removal, the SiC matrix was obtained by carbonization and siliconizing processing, and then reinforced by multilayer of carbon fibers, which caused uneven material properties with a porosity of 17%-20% in the drilling feed direction. The proportion and the distribution of SiC and carbon fibre in the drilling area is not homogeneous in all areas in the samples machining with RUD, which supports the recorded discrepancies between the simulated drilling force and actual measurements. Conversely, the measurement values also varied within a certain range and these variations are expected due to the nature of C/SiC composites. The drilling tool wear is regard as another reason for the prediction error, due to the change of the geometry and distribution of abrasives in the drilling area. In addition, the error tends to be larger at high spindle speed or high feed rate, this can be explained based on the kinematics analysis of intermittent cutting in Section 2.2. High cutting speed reduced the number of impacts per unit drilling length, and high feed rate increasing the penetration depth of abrasives, which hampered the process of chip separation from the drilling area.

5.2. Specific drilling energy analysis

The energy consumption in the drilling of C/SiC is mainly from the rotation and the feed motion of the spindle, which overcomes the resistance resulted from the axial drilling force (F) and the drilling torque (T) as marked in Fig. 7. For the RUD process, due to the resonance state with reactive power, the additional energy consumption from the vibration system is relatively small and negligible comparing the total machining energy[29,31]. And the drilling load and energy consumption are transferred to the machine spindle by the core drill, thus the drilling energy to remove the material of a hole can be expressed as:

$$e=\frac{\pi STd}{30v_f}+Fd \tag{32}$$

where d is the thickness of C/SiC workpiece and equal to 5 mm. T and F can be measured from the drilling process by dynamometer.

The volume of removed material of a hole by core drill can be considered as:

$$V=\pi((R_2+S\text{l})^2-(R_1-S\text{l})^2)d \tag{33}$$

Therefore, the drilling energy consumed for the removal of per unit volume of material, namely specific drilling energy, can be expressed as:

$$e_s=\frac{e}{V}=\frac{\pi ST+30Fv_f}{30\pi v_f((R_2+S\text{l})^2-(R_1-S\text{l})^2)} \tag{34}$$

The specific drilling energy (e_s) of CD and RUD was calculated from the measured drilling load at different drilling parameters, as shown in Fig. 11 and 12. It can be seen that the specific drilling energy increased with the spindle speed and gradually decreased with the increased of feed rate in both drilling processes, this is due to that the high rotary speed enhanced the friction between core drill and workpiece material in the closed drilling area, dissipating more drilling energy for intense friction rather than material removal, while the increase of feed rate directly reduced the drilling time of a hole, and the total friction length in the drilling area was decreased accordingly, indicating that higher portion of the energy input by spindle can be used for material removal, thus, although the drilling load was increased, the specific energy was reduced.

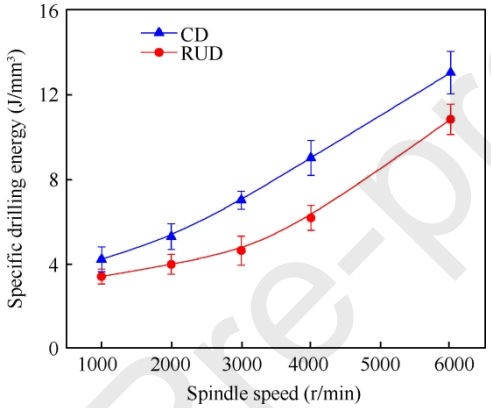

Fig. 11. Change of specific drilling energy along with spindle speed (v_f=40 mm/min).

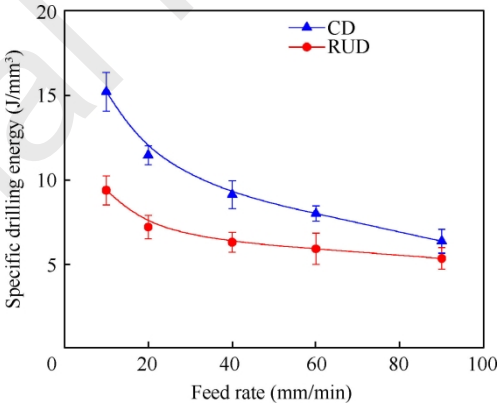

Fig. 12. Change of specific drilling energy along with feed rate (S=4000 r/min).

It was also found that the specific drilling energy of RUD was lower than that of CD on the whole. The intermittent cutting behavior significantly decreased the drilling load and avoided chip clogging, thus the energy consumed during drilling was then reduced in RUD. In addition, the ductile plowing and extrusion effect of abrasives, which generally exists in the entering stage of grinding and consume considerable machining energy with minimal material removal[34], can be suppressed by the intermittent cutting in the drilling area, this is also benefit to reduce the drilling energy dissipation in RUD. However, with the increase of spindle speed, as shown in Fig. 11, the reduction rate of specific drilling energy between RUD and CD changed from over 30% to about 15%, implying the diminishing of the effectiveness of ultrasonic vibration, similar results also observed when the feed rate increased in Fig. 12. As the kinematics discussion in Section 2, the high rotary speed reduced the number of impact per unit cutting length, while the high feed rate increased the penetration depth of abrasives in the bottom of

core drill, which may hinder the abrasives sufficiently disengaging with workpiece and achieving intermittent behavior in the drilling area. Therefore, both of these conditions will lessen the vibro-impact effect in RUD, leading to a lower reduction rate of specific drilling energy.

6. Conclusions

In this work, a fundamental investigation into RUD was carried out on ceramic matrix composites of type C/SiC. The results of the theoretical analysis and experimental studies lead to the following conclusions:

(1) The interactions between the abrasives and workpiece under ultrasonic vibration were perceived to be a compound of a vibratory lapping on cylindrical area and the impact-separation at the bottom drilling area. The equations of the motions of the abrasives were derived to characterize the effect of trajectories overlapping and intermittent cutting in different drilling areas. The high drilling speed will reduce the number of ultrasonic vibration impacts per unit cutting length, while the high feed rate, which will increase the penetration depth of abrasives, may hinder the abrasives sufficiently disengaging with workpiece and achieving intermittent behavior in the drilling area. To eliminate these diminishing effects, the equations to guarantee the effectiveness of ultrasonic vibration in RUD were then obtained.

(2) An axial drilling force model was developed for RUD based on the kinematics analysis and indentation theory. The material removal mechanism was studied, and the penetration depth of abrasives at the tool tip surface and on the flute edges were calculated respectively, taking account of the influence of flute width on cutting path. The drilling force were found to be lower and more stable in vibration assisted mode compared with the conventional drilling. This was due to the minimal volume of material removal during each vibration cycle. The prediction errors were within 15% for most of the tests, mainly due to the inhomogeneity of composites in the feed direction. The model deviation tended to slightly increase at high cutting velocity and high feed rate, because of the reduced effect of the imparted ultrasonic vibration.

(3) The specific drilling energy of RUD and CD at different drilling parameters was firstly calculated and investigated according to the measured drilling load. The intermittent cutting behavior in the drilling area, which lowered the drilling load and prevented chip clogging, can decrease the drilling energy dissipation of friction and extrusion in the closed drilling area, thus significantly reduced the specific drilling energy in RUD. Comparing with CD, the reduction rate of specific drilling energy of RUD decreased from over 30% to less than 15%, along with the increase of spindle speed and feed rate, this is due to the change of kinematics conditions leading to the diminishing of the effectiveness of ultrasonic vibration. Therefore, to achieve lower drilling force and energy consumption, the drilling parameters should be selected to match with the frequency and amplitude of ultrasonic vibration to eliminate the diminishing effects.

Acknowledgements

This work was supported by the National Natural Science Foundation of China (No. U1737201); the National Science and Technology Major Project (No. 2017-VII-0015-0111); the Key Basic and Applied Research Program of Guangdong Province, China (No. 2019B030302010); and the Science and Technology Innovation Commission Shenzhen (No. JCYJ20170412111216258).

References

1. Christin F. Design, Fabrication, and application of thermostructural composites (TSC) like C/C, C/SiC, and SiC/SiC Composites. *Adv Eng Mater* 2002;4(12):903-12.
2. Spriet P. CMC applications to gas turbines. In: Bansal NP, Lamon J, editors. *Ceramic Matrix Composites: Materials, Modeling and Technology*. Westerville: The American Ceramic Society; 2014. p. 591-608.
3. Liu X, Shen XL, Gong LD, et al. Multi-scale thermodynamic analysis method for 2D SiC/SiC composite turbine guide vanes. *Chinese J Aeronaut* 2018;31(1):117-25.
4. Schmidt S, Beyer S, Knabe H, et al. Advanced ceramic matrix composite materials for current and future propulsion technology applications. *Acta Astronaut* 2004;55(3-9):409-20.
5. Naslain R. Design, preparation and properties of non-oxide CMCs for application in engines and nuclear reactors: an overview. *Compos. Sci Technol* 2004;64(2):155-170.
6. An QL, Chen J, Ming WW, et al. Machining of SiC ceramic matrix composites: A review. *Chinese J Aeronaut* 2021:doi: 10.1016/j.cja.2020.08.001.
7. Diaz OG, Luna GG, Liao Z, et al. The new challenges of machining Ceramic Matrix Composites (CMCs):

Review of surface integrity. *Int J Mach Tools Manuf* 2019;139:24-36.
8. Diaz OG, Axinte D. Towards understanding the cutting and fracture mechanism in Ceramic Matrix Composites. *Int J Mach Tools Manuf* 2017;118-119:12-25.
9. Pei ZJ, Ferreira PM, Kapoor SG, et al. Rotary ultrasonic machining for face milling of ceramics. *Int J Mach Tools Manuf* 1995;35(7):1033-46.
10. Yuan SM, Fan HT, Amin M, et al. A cutting force prediction dynamic model for side milling of ceramic matrix composites C/SiC based on rotary ultrasonic machining. *Int J Adv Manuf Technol* 2016;86(1-4):37-48.
11. Li Z, Yuan SM, Song H, et al. A cutting force model based on kinematics analysis for C/SiC in rotary ultrasonic face machining. *Int J Adv Manuf Technol* 2018;97(1-2):1223-39.
12. Gao GF, Xia ZW, Yuan ZJ, et al. Influence of longitudinal-torsional ultrasonic-assisted vibration on micro-hole drilling Ti-6Al-4V. *Chinese J Aeronaut* 2021;doi: 10.1016/j.cja.2020.06.012.
13. Fang B, Yuan ZH, Li DP, et al. Effect of ultrasonic vibration on finished quality in ultrasonic vibration assisted micromilling of Inconel718. *Chinese J Aeronaut* 2021; doi: 10.1016/j.cja.2020.09.021.
14. Pei ZJ, Prabhakar D, Ferreira PM, et al. A mechanistic approach to the prediction of material removal rates in rotary ultrasonic machining. *J Eng Ind* 1995;117(2):142-51.
15. Zhang QH, Wu CL, Sun JL, et al. The mechanism of material removal in ultrasonic drilling of engineering ceramics. *Proc Inst Mech Eng Part B-J Eng Manuf* 2000;214(9):805-10.
16. Hu P, Zhang JM, Pei ZJ, et al. Modeling of material removal rate in rotary ultrasonic machining: designed experiments. *J Mater Process Technol* 2002;129(1-3):339-44.
17. Teti R. Machining of composite materials. *CIRP Ann Manuf Technol* 2002;51(2):611-34.
18. Hocheng H, Tai N, Liu CS. Assessment of ultrasonic drilling of C/SiC composite material. *Compos Pt A-Appl Sci Manuf* 2000;31(2):133-42.
19. Li ZC, Jiao Y, Deines TW, et al. Rotary ultrasonic machining of ceramic matrix composites: feasibility study and designed experiments. *Int J Mach Tools Manuf* 2005;45(12-13):1402-11.
20. Ding K, Fu Y, Su H, et al. Experimental studies on drilling tool load and machining quality of C/SiC composites in rotary ultrasonic machining. *J Mater Process Tech* 2014;214(12):2900-7.
21. Wang JJ, Zha HT, Feng PF, et al. On the mechanism of edge chipping reduction in rotary ultrasonic drilling: a novel experimental method. *Precis Eng* 2016;44:231-5.
22. Wang JJ, Feng PF, Zheng JZ, et al. Improving hole exit quality in rotary ultrasonic machining of ceramic matrix composites using a compound step-taper drill. *Ceram Int* 2016;42(12):13387-94.
23. Wang JJ, Feng PF, Zhang JF, et al. Reducing cutting force in rotary ultrasonic drilling of ceramic matrix composites with longitudinal-torsional coupled vibration. *Manuf Lett* 2018;18:1-5.
24. Lu YL, Yuan SM, Chen YX. A cutting force model based on kinematic analysis in longitudinal and torsional ultrasonic vibration drilling. *Int J Adv Manuf Technol* 2019;104(1-4):631-43.
25. Wang JJ, Zhang JF, Feng PF, et al. Experimental and theoretical investigation on critical cutting force in rotary ultrasonic drilling of brittle materials and composites. *Int J Mech Sci* 2018;135:555-64.
26. Dong GJ, Lang CY, Li C, et al. Formation mechanism and modelling of exit edge-chipping during ultrasonic vibration grinding of deep-small holes of microcrystalline-mica ceramics. *Ceram Int* 2020;46(8):12458-69.
27. Li C, Zhang FH, Meng BB, et al. Material removal mechanism and grinding force modelling of ultrasonic vibration assisted grinding for SiC ceramics. *Ceram Int* 2016;43(3):2981-93.
28. Li C, Li XL, Wu YQ, et al. Deformation mechanism and force modelling of the grinding of YAG single crystals. *Int J Mach Tools Manuf* 2019;143:23-37.
29. Cong W, Pei ZJ, Deines TW, et al. Rotary ultrasonic machining of CFRP composites: a study on power consumption. *Ultrasonics* 2012;52(8):1030-37.
30. Islam S, Yuan SM, Li Z. Mathematical modeling and experimental studies on axial drilling load for rotary ultrasonic drilling of C/SiC composites. *Int J Adv Manuf Technol* 2020;107:1309-26.
31. Batako AD, Morgan MN, Rowe B. High efficiency deep grinding with very high removal rates. *Int J Adv Manuf Technol* 2013;66(9-12):1367-77.
32. Marshall DB, Lawn BR, Evans AG. Elastic/plastic indentation damage in ceramics: the lateral crack system. *J Am Ceram Soc* 1982;65(11):561-6.
33. Lankford J. Indentation microfracture in the Palmqvist crack regime: implications for fracture toughness evaluation by the indentation method. *J Mater Sci* 1982;1:493-5.
34. Malkin S, Guo CS. *Grinding Technology: Theory and applications of machining with abrasives*. New York: Industrial Press Inc.; 2008. p. 115-20.